

Application of the NCEP Regional Spectral Model to Improve Mesoscale Weather Forecasts in Hawaii

JIAN-JIAN WANG*

UCAR COMET Outreach Program, Boulder, Colorado

HANN-MING HENRY JUANG

EMC/NCEP, Washington, D.C.

KEVIN KODAMA⁺

Joint Institute for Marine and Atmospheric Research, Honolulu, Hawaii

STEVE BUSINGER AND YI-LENG CHEN

University of Hawaii at Manoa, Honolulu, Hawaii

JAMES PARTAIN[#]

National Weather Service, Pacific Region, Honolulu, Hawaii

(Manuscript received 23 April 1997, in final form 14 October 1997)

ABSTRACT

The operational implementation of the National Centers for Environmental Prediction (NCEP) Regional Spectral Model (RSM) in Hawaii is the first application of a mesoscale model to improve weather forecasts in the Pacific region. The primary model guidance for the National Weather Service Pacific region has been provided by the NCEP Aviation (AVN) run of the Global Spectral Model (GSM). In this paper, three recent synoptic-scale disturbances that affected the Hawaiian Islands are selected to demonstrate the potential utility of model guidance produced by the RSM and contrast it qualitatively with that from the AVN. NCEP RSM simulations, with enhanced grid resolution, can resolve convective rainbands and the interaction between the environmental airflow and the complex island topography, features the GSM cannot capture.

RSM model performance in reproducing mesoscale structures associated with the synoptic-scale systems is encouraging. For the first simulation, a kona low case on 3 November 1995, the RSM predicted a northeast-southwest-oriented rainband that closely matched a convective cloud band in the satellite imagery and maximum rainfall over Kauai. The second RSM simulation, a cyclogenesis event on 3 March 1996, shows remarkable agreement with observations. Important features such as the heavy rains and high winds over portions of Maui and Hawaii are accurately forecast. The third RSM simulation, a heavy rain event on 13 November 1996, is associated with convergence along a trailing cold-frontal trough. In this case the RSM correctly forecast the timing and distribution of heavy rainfall on the island of Oahu. Subjective comparisons between RSM output and observations demonstrate the potential utility of the model guidance for local weather forecasts in Hawaii.

1. Introduction

Throughout most of the year, the Hawaiian Islands benefit from the mild conditions characteristic of the trade wind regime. Comfortable temperatures and humidities as well as gentle breezes contribute to the popularity of the island chain for both residents and visitors alike. However, violent weather associated with synoptic- and mesoscale disturbances occurs with surprising frequency. From 1970 to 1990, the National Weather Service (NWS) reported an average of six flash floods

* Current affiliation: Department of Atmospheric Sciences, University of Illinois at Urbana-Champaign, Urbana, Illinois.

⁺ Current affiliation: Forecast Office, National Weather Service, Honolulu, Hawaii.

[#] Current affiliation: MPC/NCEP, Washington, D.C.

Corresponding author address: Dr. Jian-Jian Wang, Department of Atmospheric Sciences, University of Illinois at Urbana-Champaign, 105 South Gregory Street, Urbana, IL 61801-3070.
E-mail: jjwang@uiuc.edu

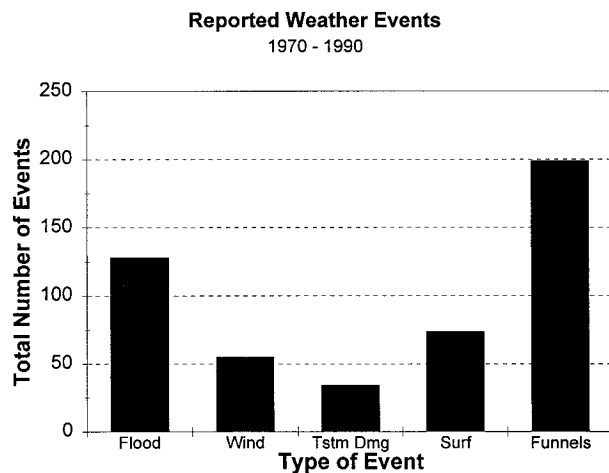


FIG. 1. Statistics report of weather events during the period of 1970–90. *Tstm Dmg* includes all reports of damage caused by thunderstorm activity other than floods (e.g., convective gusts, lightning, and hail). *Funnels* includes all reports of tornadoes, waterspouts, and funnel clouds.

per year (Fig. 1) and numerous high wind events ($>20 \text{ m s}^{-1}$), causing casualties (69 in all) and severe property damage (e.g., the January 1980 flood on Maui resulted in $>\$50$ million damage). During the month of November 1996, the Waianae coast of Oahu received more than 600 mm (2 ft) of rain from extratropical systems, an amount equal to the annual average rainfall, triggering flash floods and landslides that sent mud and rocks into

the second story of a Makaha condominium complex on 14 November 1996.

Most Hawaiian storms are related to one of four classes of synoptic-scale disturbances: cold fronts, kona lows, upper tropospheric troughs, and tropical cyclones (Fig. 7 in Kodama and Businger 1998). Although weather patterns in the Hawaiian Islands can be broadly characterized by synoptic-scale patterns, weather hazards are primarily organized on the mesoscale and the impact of terrain is critical in determining the severity of local conditions. For the eight major islands in the chain (Hawaii, Maui, Kauai, Oahu, Molokai, Lanai, Kahoolawe, and Niihau), this terrain is mountainous and complex, consisting of active and extinct volcanoes. Noteworthy is the fact that 50% of the land is above 2000 ft (610 m) (Blumenstock and Price 1967). The volcanoes of the western islands (i.e., Kauai and Oahu) are extinct and heavily eroded, with amphitheater-like valleys cut deep into the slopes. The summit elevations here are from 1 to 2 km. In contrast, the eastern islands of Maui and Hawaii consist of massive, active volcanoes with relatively gentle slopes and summit elevations as high as 4.1 km.

Observational studies (e.g., Haraguchi 1977; Kodama and Barnes 1997) clearly show the effects of the terrain on the distribution of heavy rainfall in the Hawaiian Islands. Even during times of low wind speeds or light to moderate trade winds the thermal and dynamic effects of the island topography results in orographic clouds and precipitation (e.g., Leopold 1949; Garrett 1980; Smolarkiewicz et al. 1988). Recent analyses of the Ha-

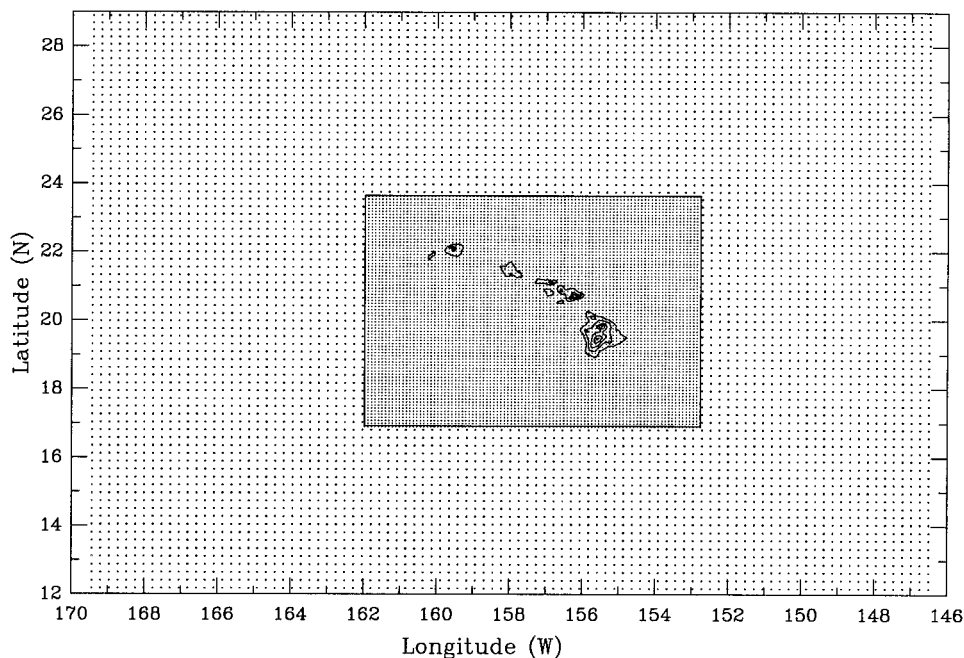
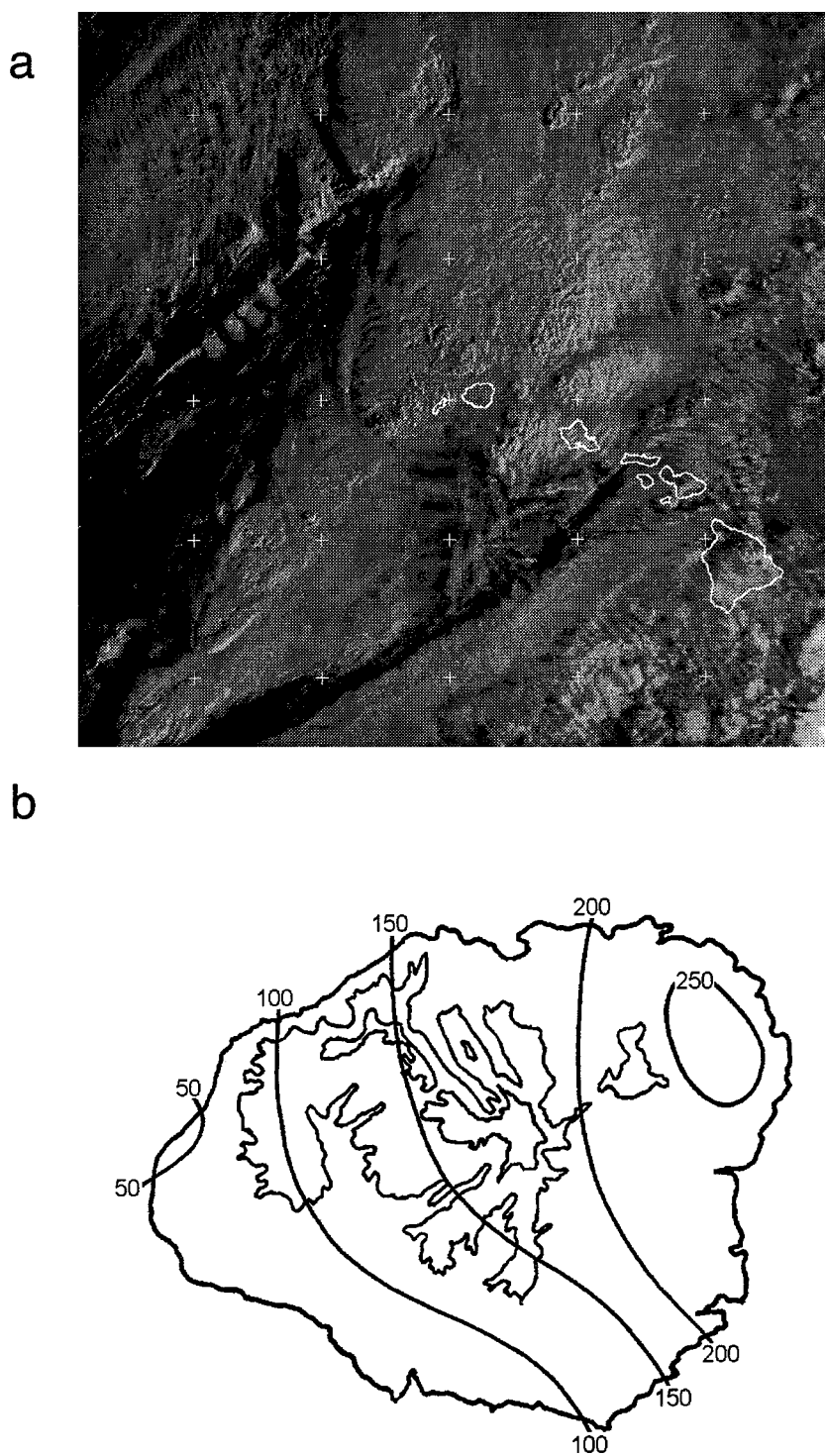


FIG. 2. Hierarchy of the nested RSM. The resolution is 25 km for the outer domain and 10 km for the middle domain. The contour interval of the Hawaiian Islands topography is 1000 m.



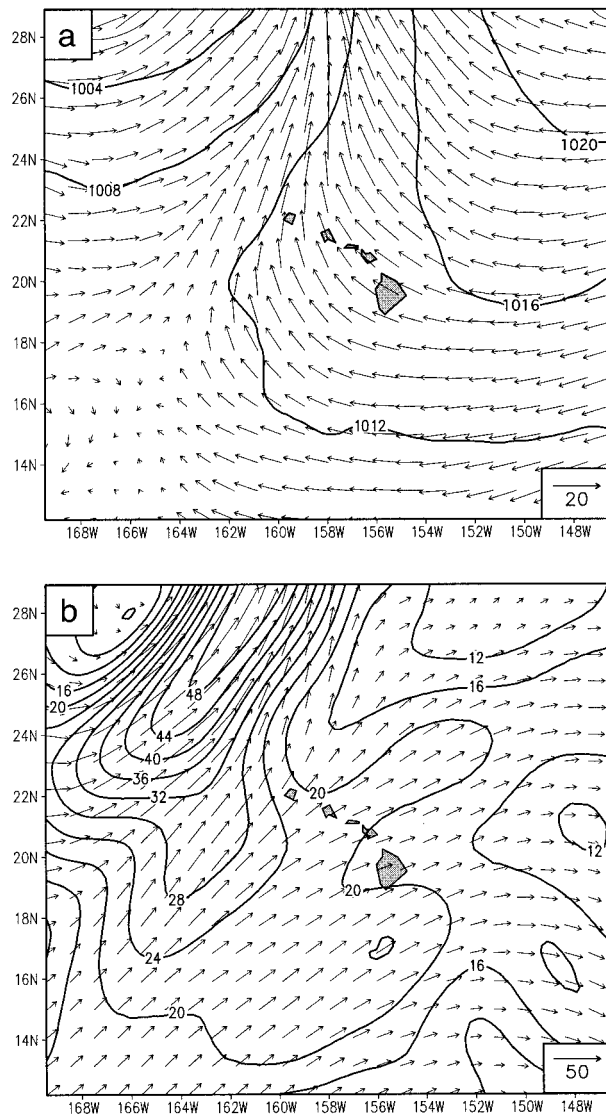


FIG. 4. AVN 24-h forecast valid at 0000 UTC 4 November 1995: (a) sea level pressure (hPa) and 1000-hPa wind vectors ($m s^{-1}$); (b) 250-hPa wind vectors and isotachs ($m s^{-1}$).

waiian Rainband Project (HaRP 1990) data have provided a better understanding of the orographic effects and the diurnal variations of local airflow and rainfall (Chen and Nash 1994). The interaction between the trade wind rainbands and island-induced circulations plays an important role in the evolution of early morning rainbands as they move onshore (Wang and Chen 1998). In turn, the distributions of clouds and precipitation affect thermal fields and airflow (Chen and Wang 1994, 1995; Wang and Chen 1995).

Operational forecasters in Hawaii use the Aviation (AVN) run of the Global Spectral Model (GSM) from the National Centers for Environmental Prediction (NCEP) as the primary model guidance for 0–78-h forecasts. Its 1° model output resolution is generally able

to provide a reasonable representation of the synoptic-scale environment. However, the highly localized nature of Hawaiian heavy rain and high wind events cannot be simulated by the AVN due to its coarse resolution and its poor representation of the complex, mountainous terrain that defines the island chain.

An adaptation of the high resolution NCEP Regional Spectral Model (RSM) (Juang and Kanamitsu 1994) is now available for the Pacific region of the NWS and is expected to provide much better numerical guidance than the AVN for operational forecasts of the local weather. This paper presents the results of high-resolution (nested to 10 km) RSM simulations for three cases of heavy rain and high winds associated with a kona low and two cold frontal passages. Although the simulation of a tropical cyclone is not considered in this paper, the RSM may improve hurricane track guidance and local impact forecasts should a hurricane affect Hawaii in the future.

The general characteristics of the NCEP RSM and its design for Pacific region applications are described in section 2. Three case studies are presented in section 3, and a summary and conclusions are given in section 4.

2. RSM model description and design

A comprehensive description of the NCEP RSM is available in Juang and Kanamitsu (1994). Therefore, we limit ourselves to a brief description of its basic formulation and its adaptation to Hawaii in this section. The primitive equations in sigma coordinates used in the global spectral model (GSM) are applied in the RSM. While the GSM uses spherical harmonics functions, the RSM uses sine or cosine series as horizontal basis functions in a Mercator projection over Hawaii. The dependent variables in the regional domain are divided into a time-dependent base field and a perturbation part in terms of their spectral representation. The RSM then predicts deviations from the forecast of the global model component. In other words, the RSM can resolve and predict those features not predicted in the GSM. A semi-implicit adjustment is applied to those deviations in the regional domain to permit numerical stability with a larger time step.

To maintain consistency between the global and the regional models, the same 28-layer model physics as in the GSM are used in the RSM computation. The model physics includes short- and longwave radiation with diurnal variation, radiation–cloud interaction, a surface layer with planetary boundary layer physics, gravity-wave drag, simplified Arakawa–Schubert convective parameterization scheme, shallow convection, large-scale precipitation, and some hydrological processes (Kanamitsu 1989). To further reduce noise from the lateral boundaries, a lateral boundary relaxation is also performed on the total tendency computed in the RSM. A time filter (Asselin 1972) is applied to the perturbations

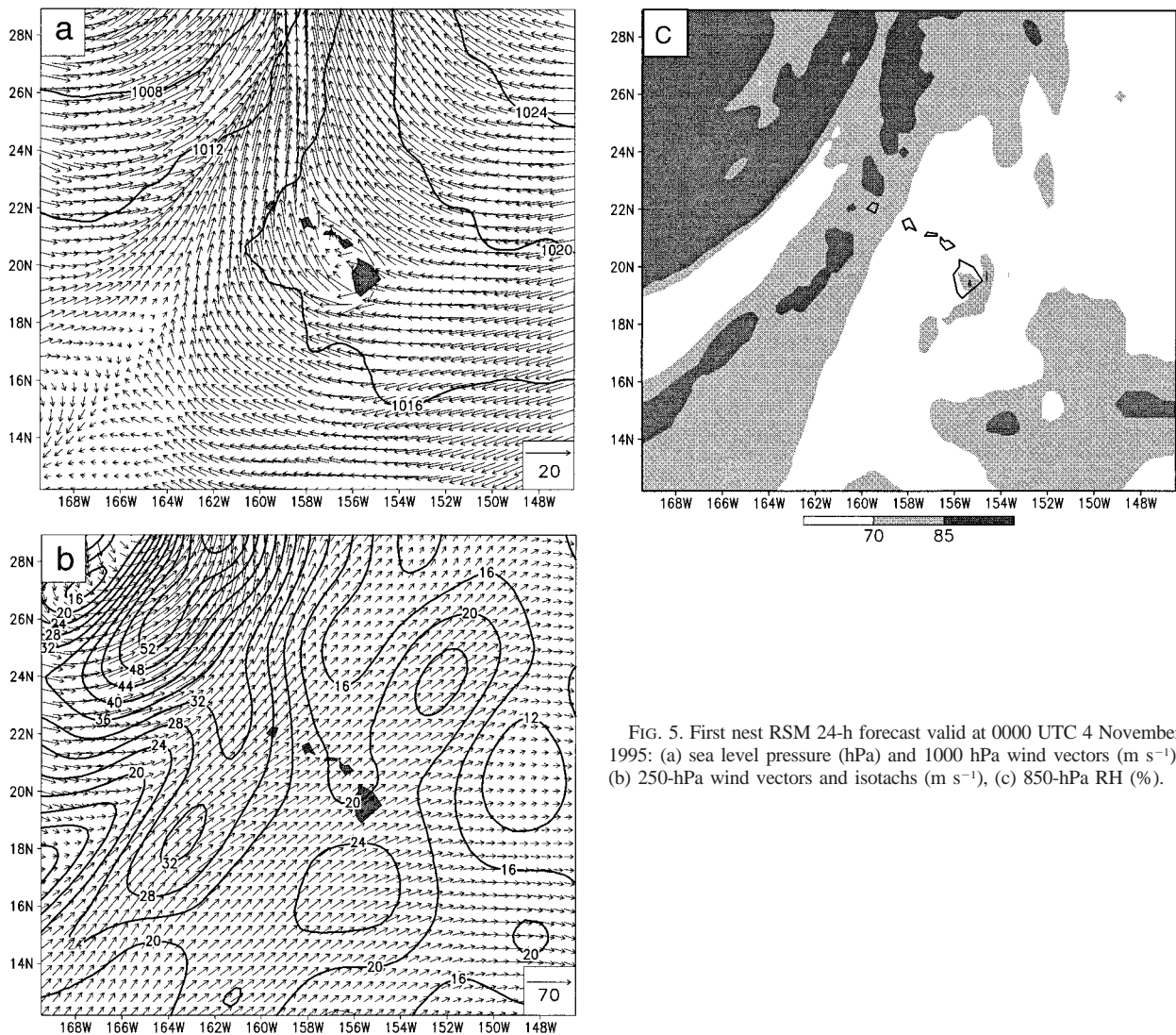


FIG. 5. First nest RSM 24-h forecast valid at 0000 UTC 4 November 1995: (a) sea level pressure (hPa) and 1000 hPa wind vectors (m s^{-1}); (b) 250-hPa wind vectors and isotachs (m s^{-1}), (c) 850-hPa RH (%).

in order to eliminate the computational mode resulting from a leapfrog time scheme in the integration.

The current implementation of the RSM is hydrostatic; a nonhydrostatic version is currently undergoing tests at NCEP (Juang 1996). Generally, observed vertical velocities in thunderstorm updrafts in the Tropics are much weaker ($<10 \text{ m s}^{-1}$) than those observed over midlatitude land masses (Jorgensen and LeMone 1989). Therefore, a hydrostatic version of the RSM should be sufficient to describe general patterns.

The entire system designed for Hawaii consists of three components (Fig. 2): the GSM, the first nest of the RSM, and the second nest of the RSM. The GSM component is a version of the operational NCEP Global Spectral Model at 106-km resolution. A 97×76 -point grid domain is used for both the first and second nests of the RSM. The first RSM nest, at 25-km resolution

and a time step of 180 s, covers a synoptic-scale domain of $2400 \times 1875 \text{ km}$ centered over Hawaii, while the second RSM nest, at 10-km resolution and a time step of 80 s covers a mesoscale domain of $960 \times 750 \text{ km}$ over the major Hawaiian Islands. High-resolution (1 km) terrain data (Navy-NCAR) for the Hawaiian Islands are used in the model. Since the RSM has the same physics as the GSM, the initial conditions and lateral boundary conditions for the first RSM nest are obtained from a T126 NCEP GSM run, which uses a spectral statistical interpolation analysis. Subsequently, the output from the first RSM nest provides the initial conditions and lateral boundary conditions for the second RSM nest.

The RSM simulations presented in this paper were run on a Digital Equipment Corporation (DEC) AlphaServer 2100 workstation in the Department of Meteorology at the University of Hawaii. The RSM out-

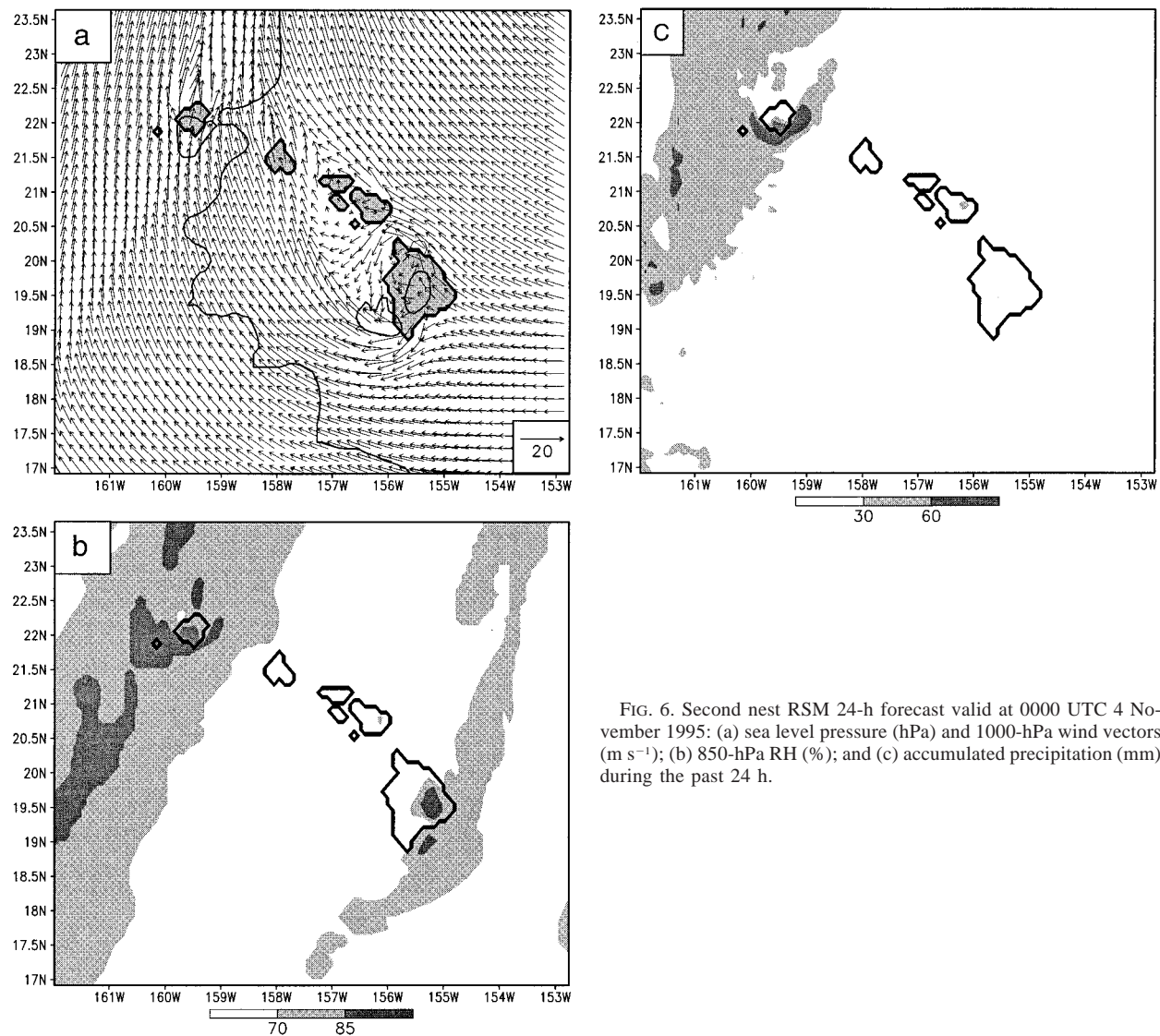


FIG. 6. Second nest RSM 24-h forecast valid at 0000 UTC 4 November 1995: (a) sea level pressure (hPa) and 1000-hPa wind vectors (m s^{-1}); (b) 850-hPa RH (%); and (c) accumulated precipitation (mm) during the past 24 h.

put is directly networked to the NWS Forecast Office, Honolulu, which is collocated with the Department of Meteorology at the University of Hawaii.

3. Case studies

a. Kona low of 3–4 November 1995

During the late morning hours of 3 November 1995, a line of thunderstorms with a northeast–southwest orientation brought heavy rainfall to most of the island of Kauai (Fig. 3a). Between 1700 UTC (0700 Hawaiian Standard Time; HST) 3 November and 1700 UTC 4 November, the north and east sides of the island recorded rainfall of 200–250 mm, while the south and west sides of the island received 50–100 mm of rain (Fig. 3b). The heavy rain caused several areas of flooding from the northern through eastern portions of the

island, resulting in road closures and evacuations. Low ceilings, poor visibility, and erratic winds during the event resulted in the cancellation of 17 flights between the island of Kauai and Oahu. Monetary losses from the flooding were estimated at \$685,000.

In the upper troposphere, a cold low pressure system centered around 31°N , 168°W becomes cut off from the westerlies (Fig. 1 in Businger et al. 1998). Associated surface cyclogenesis is consistent with a class of subtropical cyclones known as kona lows (Simpson 1952; Ramage 1962; Schroeder 1977). The surface analyses during the period from 0000 UTC 3 November to 0000 UTC 4 November show a relatively stationary low pressure system centered near 34°N , 165°W (Fig. 2 in Businger et al. 1998). Under this synoptic situation, the islands of Kauai and Oahu were in a region of convergent southerly flow, whereas the islands of Hawaii and Maui were under the influence of easterly trade winds.

The GSM and RSM simulations for this case were initialized at 0000 UTC 3 November 1995, ~24 h prior to the heaviest rainfall. In general, the 24-h AVN forecast at 0000 UTC 4 November was reasonably accurate in describing the synoptic-scale features near the Hawaiian Islands. The surface low and a low-level convergence zone are located northwest of the islands, whereas the trade winds prevail across the eastern domain (Fig. 4a), consistent with ship observations (Fig. 2 in Businger et al. 1998). At 250 hPa (Fig. 4b), a strong circulation with maximum winds of 45–50 m s⁻¹ is seen around a cold low aloft northwest of Kauai. In the right jet entrance region, upper-level diffluence is present over the Hawaiian Islands (Uccellini and Johnson 1979). Aside from the synoptic-scale features, the result of limited resolution of the AVN on the accuracy of the forecast near the islands is apparent. The AVN forecast did not resolve island-induced phenomena, such as orographic deformation of the wind field and precipitation enhancement.

The first nest of the RSM was used to produce a 24-h forecast initializing at 0000 UTC on 3 November 1995 (Fig. 5). At 0000 UTC 4 November, the 1000-hPa winds (Fig. 5a) displayed southwesterlies in the northwestern area and southeasterlies to the south of the Hawaiian Islands. In this figure, and others in this paper, in which the atmospheric pressure level intersects the island terrain, the data represent near-surface conditions or lowest-level data over the model terrain. Low-level wind field exhibited mesoscale features induced by the island topography, such as flow splitting around the islands of Hawaii and Maui, as well as the confluence in the lee side of the island of Hawaii (Fig. 5a). In the upper troposphere, the primary jet stream, with a maximum wind speed of 55 m s⁻¹, was located in the northwest corner of the domain. In addition, there was a secondary jet centered at 18.2°N, 163.7°W, with a maximum wind speed of 33 m s⁻¹. This secondary jet, developing from 1200 UTC 3 November to 0000 UTC 4 November, was not predicted by the AVN. When the heavy rainfall occurred, Kauai was on the left side of the jet exit region, providing upper-divergence conducive to the development of heavy rainfall. In summary, both the low-level and upper-level conditions predicted by the first nest of the RSM were supportive for the development and maintenance of deep convection. Two bands of greater than 80% relative humidity (RH) at 850 hPa were forecast, one in the northwestern corner of the domain and the other oriented northeast–southwest and covering Kauai (Fig. 5c). These two bands of high RH match the two

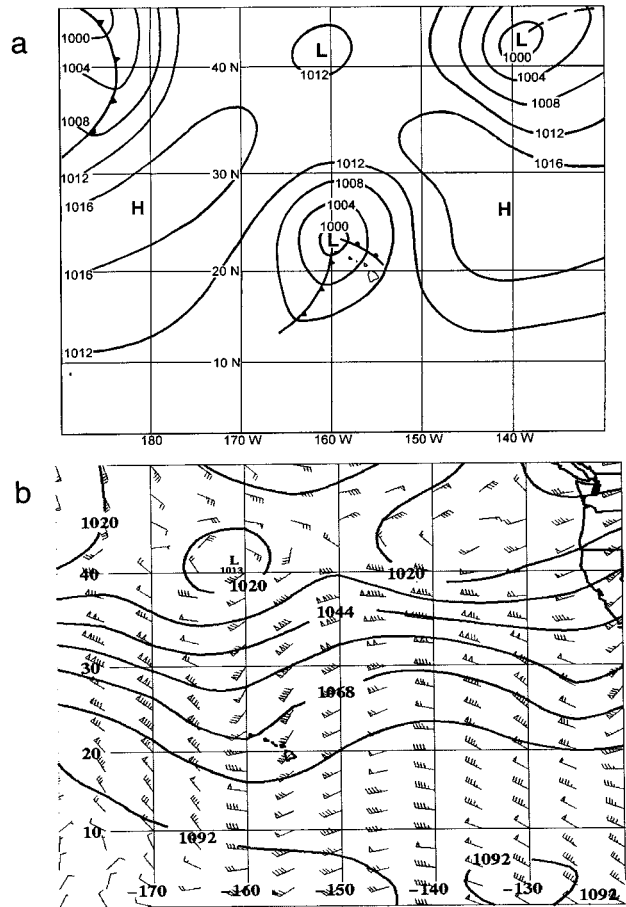
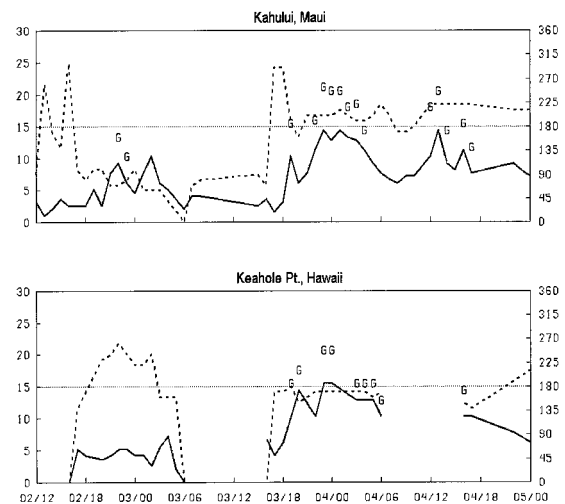
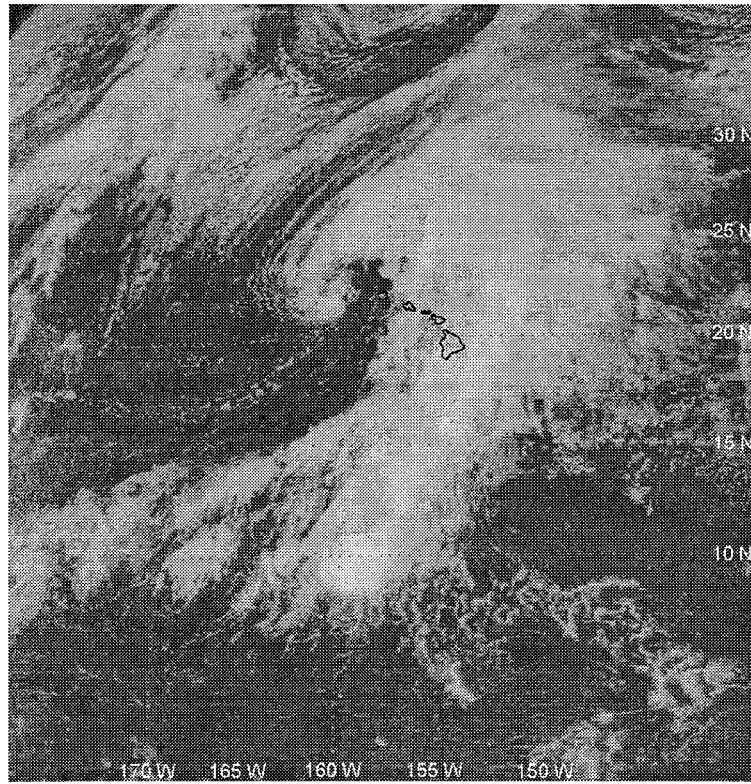


FIG. 7. (a) Surface chart at 0000 UTC 4 March 1996, isobars are plotted for every 4 hPa (adapted from the subjective analysis by forecasters at the National Weather Service Forecast Office, Honolulu); (b) 250-hPa geopotential height (dam) and winds (m s⁻¹), conventional wind barbs (pennants = 25 m s⁻¹, long bars = 5 m s⁻¹, and short bars = 2.5 m s⁻¹); (c) GOES visible wavelength satellite image from 2330 UTC 3 March 1996; (d) 24-h accumulated precipitation from 1700 UTC 2 March to 1700 UTC 3 March 1996.

FIG. 8. Meteograms from 1200 UTC 2 March to 0000 UTC 5 March 1996 at Kahului, Maui (top panel), and Keahole Point, Hawaii (bottom panel). Solid lines depict wind speeds (m s⁻¹), dashed lines indicate wind direction (°), and the letter “G” indicates magnitude reported wind gusts (m s⁻¹). The wind speed and gust scale is on the left, and the wind direction scale is on the right.



c



d

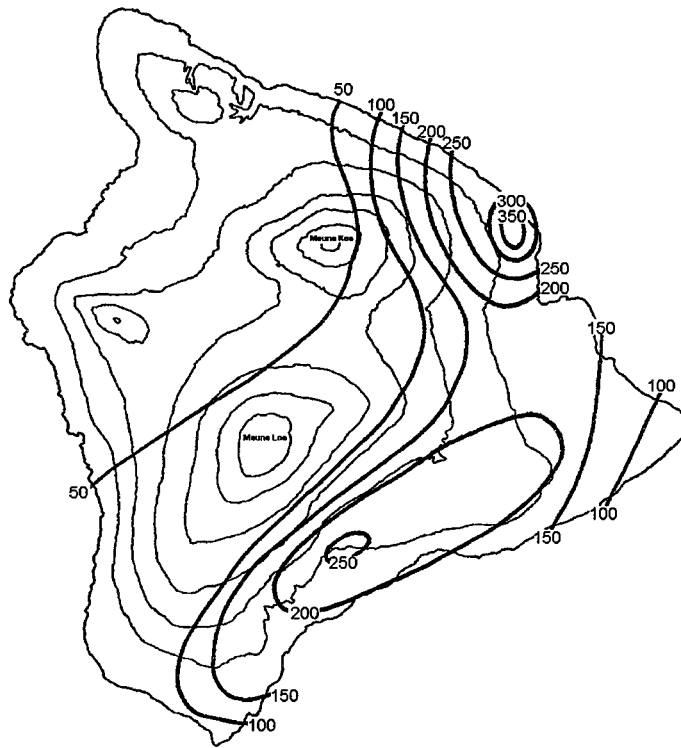


FIG. 7. (Continued)

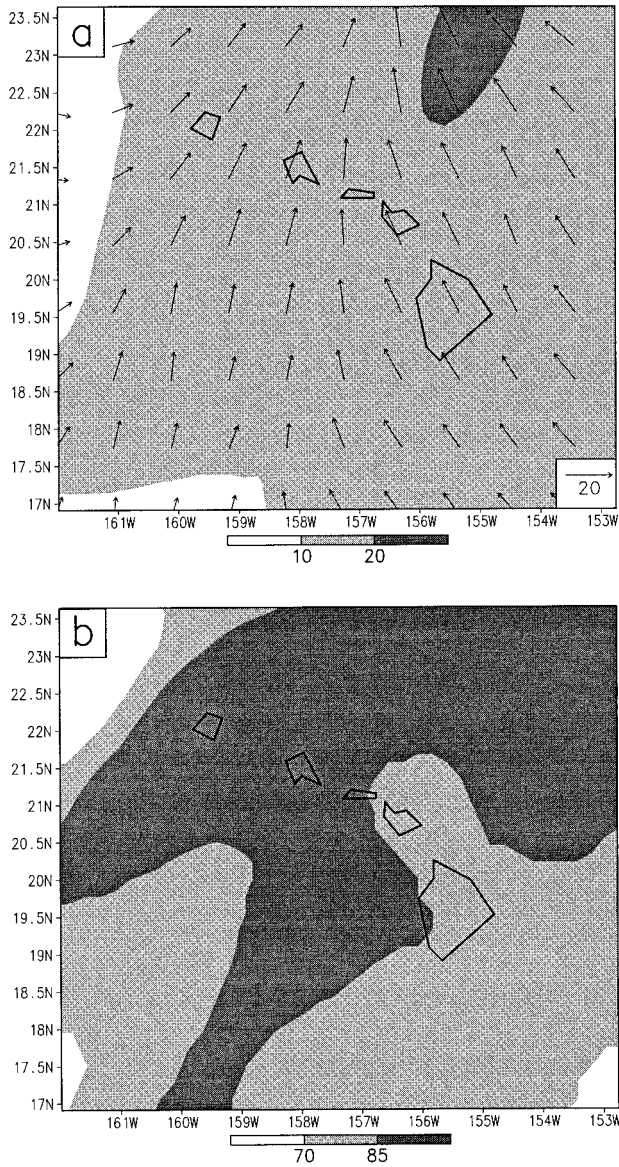


FIG. 9. AVN 24-h forecast valid at 0000 UTC 4 March 1996: (a) 1000-hPa winds (m s^{-1}); (b) 850-hPa RH (%).

principal cloud bands in the satellite image at that time very well (Fig. 3a). The GSM failed to reproduce these features (not shown).

The 24-h forecasts produced by the second nest of the RSM and valid at the same time (0000 UTC 4 November) are summarized in Fig. 6. The second RSM nest resolves considerably more detail of the local circulation patterns (Fig. 6a). Airflow was affected not only by the larger and higher islands of Hawaii and Maui, but also by the smaller and lower islands Oahu and Kauai. The 850-hPa RH from the second RSM nest (Fig. 6b) displays details over the islands not resolved by the first RSM nest. A band of high RH surrounding the island of Kauai and a localized maximum ($>85\%$) just

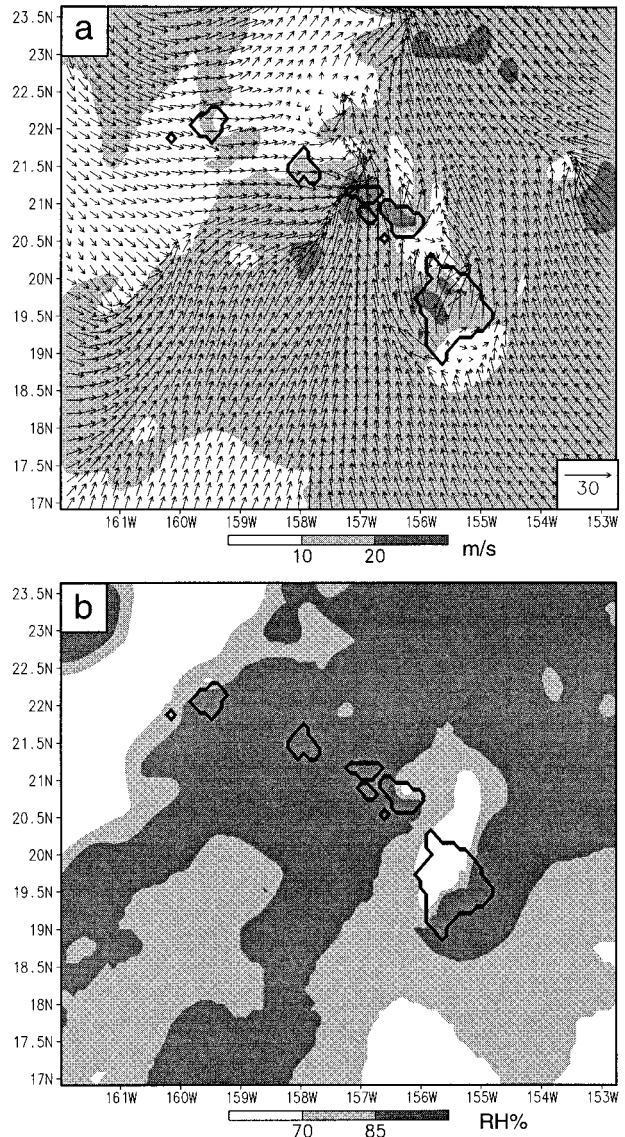


FIG. 10. Second nest RSM 24-h forecast valid at 0000 UTC 4 March 1996: (a) 1000-hPa winds (m s^{-1}), (b) 850-hPa RH (%), and (c) accumulated precipitation (mm) during the past 24 h.

over the island correlates with the model-predicted heavy rainfall (Fig. 6c). A localized RH maximum is also forecast on the windward slopes of the island of Hawaii. As found by Chen and Wang (1994), this area of high RH is consistent with a diurnal phenomenon in the afternoon hours (0000 UTC = 1400 HST) at that location, where the combination of trade winds and sea breeze moves upslope (Chen and Nash 1994). The afternoon upslope flow may cause showers over the slopes but usually results in small 24-h rain amounts (Fig. 6c). Simulations of other cases of weak synoptic forcing confirm the RSM's general ability to forecast these features. This is a subject that will be explored further in future research.

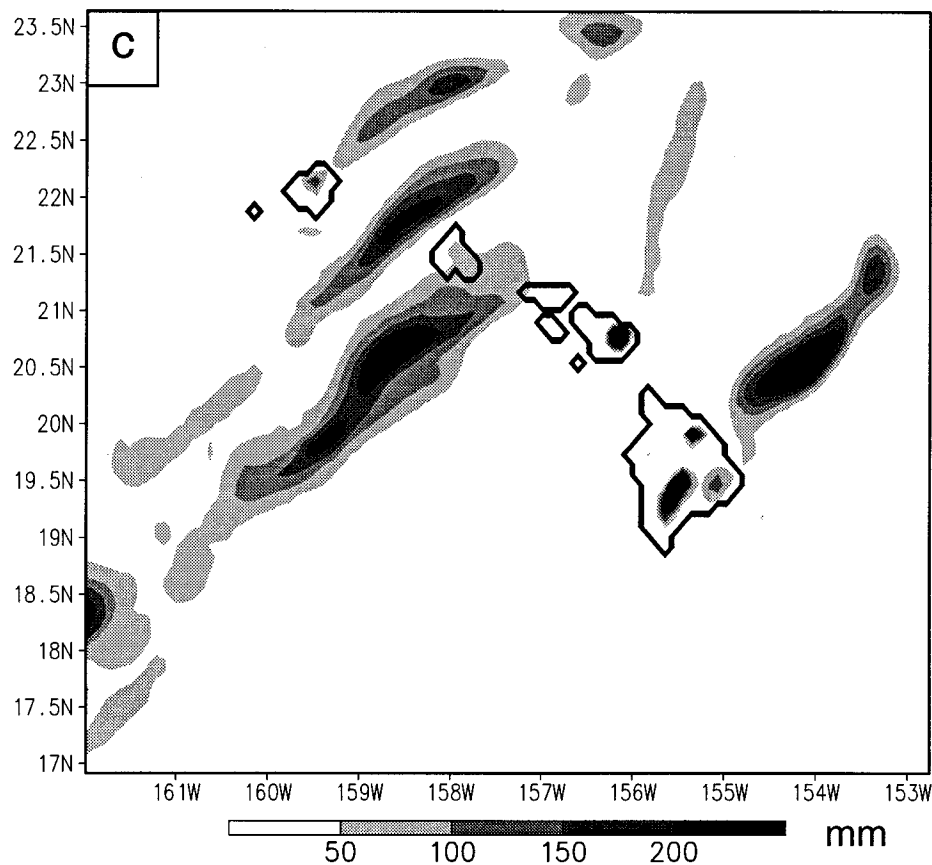


FIG. 10. (Continued)

The 24-h accumulated precipitation forecast from 0000 UTC 3 November to 0000 UTC 4 November by the second RSM nest showed a northeast–southwest rainband over Kauai with a maximum of 70 mm over the southern side of the island. Compared with the rainfall observations (Fig. 3b), the RSM successfully forecast the occurrence of heavy rainfall over Kauai. However, the rainfall amount predicted by the RSM was about one-third that observed. In addition, the area of heavier rainfall is forecast over the southern half of the island, whereas observations show the maximum rainfall occurred over the northeastern section of the island.

Most heavy rainfall events occur on the windward side of the island. However, this case was an exception. Both the RSM forecast (Fig. 4a) and surface map (Fig. 2 in Businger et al. 1998) showed southwesterly winds in the lowest levels around the island while the heavy rainfall was recorded on the northeastern side of the island. The location of the flood for this case may be related to the flow interaction with the local complex terrain. This interaction probably involves local-scale and nonhydrostatic processes (Wang and Chen 1995), which are not well handled by the hydrostatic RSM at a resolution of 10 km. The total accumulated precipitation was also underpredicted by the RSM for this case

and may reflect inadequacies of the current precipitation scheme in simulating the physical processes governing the production of heavy rainfall in the Hawaiian Islands. A new precipitation physics package is being tested at NCEP (Hong and Juang 1996) and it is anticipated that these improvements will provide better precipitation forecasts in the near future.

Nevertheless, the RSM output provided much better 24-h forecast guidance than the AVN for this heavy rainfall event on Kauai. The RSM performed reasonably well in predicting the mesoscale environmental conditions and occurrence of heavy rainfall in the vicinity of Kauai.

b. Cyclogenesis event of 2–4 March 1996

During the period of 2–4 March 1996, a wave developed on a stationary front northwest of Hawaii and moved northeast at 7 m s^{-1} , producing heavy rains and high winds across most of the island chain. Although heavy rains affected the entire state, the highest amounts and worst flooding occurred during the morning hours of 3 March over the southeastern half of the island of Hawaii. Rain along the northeastern coastline resulted in several spot evacuations and induced landslides that

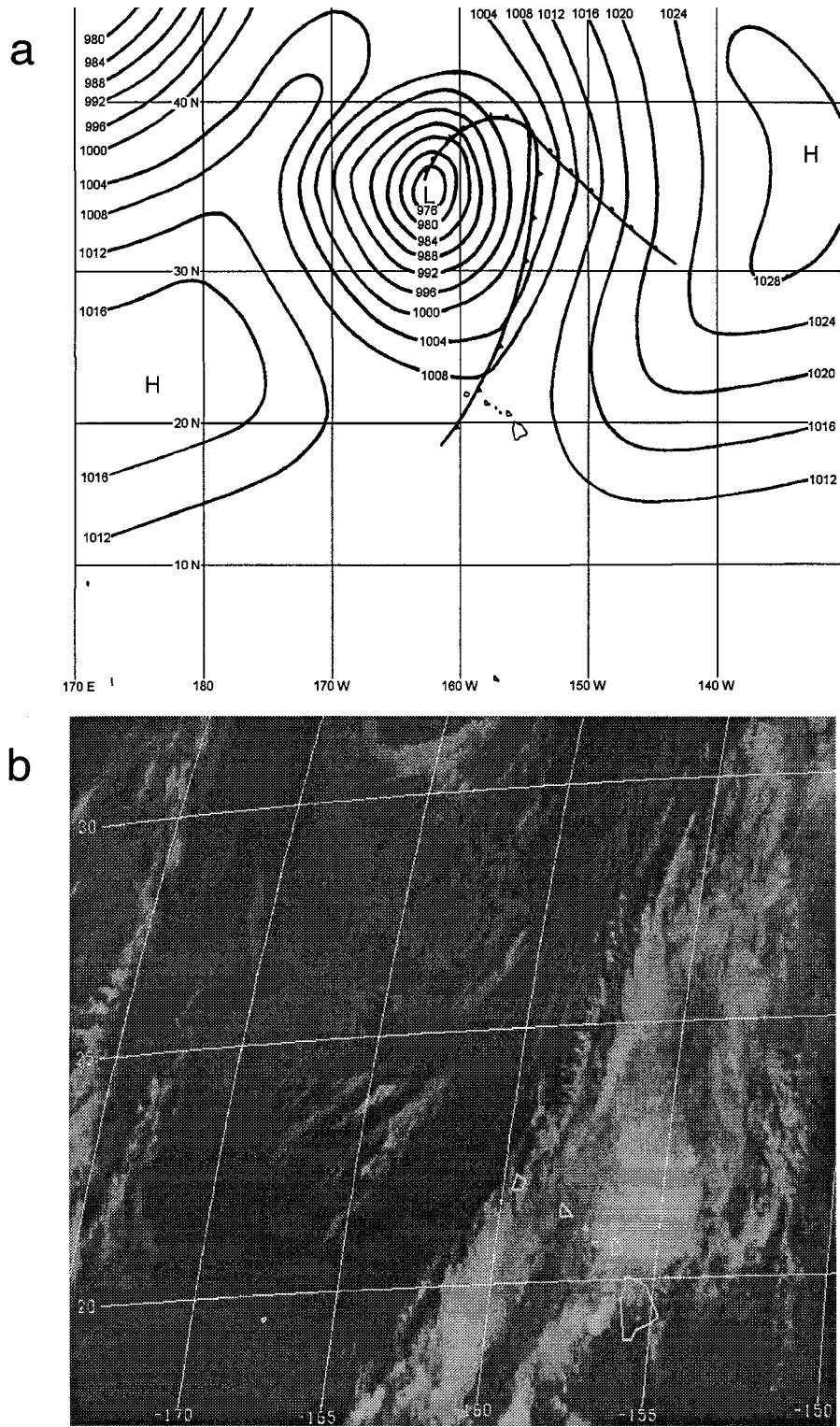


FIG. 11. (a) Surface chart at 0000 UTC 14 November 1996 (adapted from the hand-drawn analysis by forecasters at the NWSFO, Honolulu). Surface chart isobars are plotted for every 4 hPa. (b) GOES infrared wavelength satellite image at 0000 UTC 14 November 1996. (c) 24-h accumulated precipitation from 1700 UTC 12 November to 1700 UTC 13 November 1996. Rainfall isopleths are in millimeters.

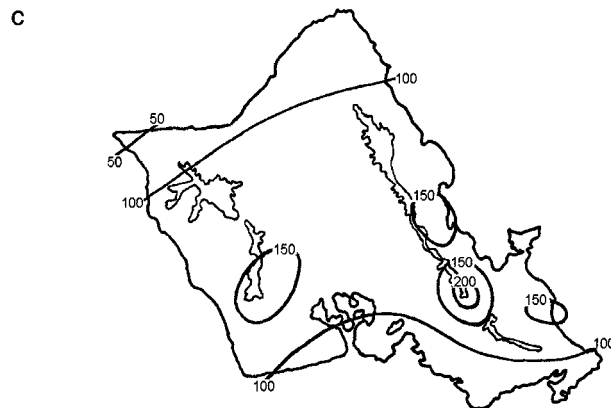


FIG. 11. (Continued)

closed the main “belt” highway for several hours. Concurrently, flooding over the southeastern slopes inundated portions of the belt highway with 6 ft of water. Strong winds followed the rains on 3 and 4 March. Numerous structures suffered varying degrees of damage and downed power lines disrupted electrical service across the state. On the island of Maui, high winds cut electrical service to over 40% of the island. Strong coastal winds also cut several boats free from their moorings on the islands of Maui and Hawaii. Gusts in excess of 45 m s^{-1} atop Haleakala volcano on the island of Maui damaged all radio and television transmitters, resulting in the loss of service through 4 March.

The surface analysis for 0000 UTC 4 March 1996 (Fig. 7a) shows a mature surface low centered at 23°N , 160°W northwest of Kauai with a minimum pressure of 998 hPa. The cyclone evolved from a wave on a front that stalled just northwest of the Hawaiian Islands on March 2 in response to the approach of an upper-level trough from the northwest (Fig. 7b). *GOES-9* visible imagery shows an asymmetric cloud shield of the mature midlatitude cyclone, located at relatively low latitudes in this case (Fig. 7c). During the period 1700 UTC 2 March to 1700 UTC 3 March 1996, over 200 mm of rain fell on portions of the southeastern half of the island of Hawaii (Fig. 7d). In contrast, the northwestern side of the island experienced less than 50 mm of rainfall during the same period. The onset of high winds followed the heavy rains on all of the islands except Kauai. Around 0000 UTC 4 March, stations at Kahului, Maui, and Keahole Point, Hawaii, observed southerly winds, with gusts in excess of 20 m s^{-1} (Fig. 8).

The 24-h model simulation of this case was initialized at 0000 UTC 3 March 1996. In this case the AVN 24-h forecast again provides an adequate simulation of the synoptic conditions. A surface low was forecast to the northwest of the Hawaiian Islands (Fig. 9a). East of the surface low and downstream of the upper-tropospheric trough was a band of high RH in the low levels that covered the western part of the Hawaiian Islands. As in the previous kona low case, the AVN simulation was

unable to resolve the effects of the island topography and did not provide sufficient guidance for localized weather conditions. The winds at 1000 hPa showed relatively uniform wind speed ($12\text{--}16 \text{ m s}^{-1}$) through the islands (Fig. 9a), less than observed on Maui and Hawaii (Fig. 8). The 24-h low-level RH forecast for the island of Hawaii was also poor (Fig. 9b). On the southern and eastern portions of the island, where flooding occurred, low RH ($<85\%$) values were predicted. The only area with high RH ($>85\%$) over the island was on the western coast, where the observed 24-h rainfall was less than 50 mm.

In contrast to the AVN run, the second nest RSM simulation provides much more accurate guidance on local weather for this weather event. The speed of the large-scale southeasterly flow decreases significantly as it approaches the island with splitting airflow off the southeastern coast. These features are the result of island blocking for a low-Froude-number (<1) flow regime. Using Hilo sounding data for 3 March, the Froude number was ~ 0.4 , corresponding to a wind speed of 15 m s^{-1} , a Brunt-Väisälä frequency of 0.0014 s^{-1} , and a mountain height of 2700 m (e.g., Smolarkiewicz et al. 1988). High winds are simulated in the Kona and Hilo areas as the low-level airflow moves around the island topography. On the southeastern flank of Mauna Loa, orographic lifting is evident with high RH there (Fig. 10b). On the northern and northwestern sides of the island, RH is less than 70% suggesting sinking motion over the lee side of the mountains under the prevailing southeasterly flow. Southwesterly flow west of Molokai converges with southerly flow south of Maui with simulated high winds over Molokai and western Maui.

The 24-h precipitation forecast (0000 UTC 3 March–0000 UTC 4 March 1996) by the second RSM nest showed three heavy rainfall centers ($>200 \text{ mm}$): (i) eastern Maui, (ii) the southeastern flank, and (iii) the northeast coast of the island of Hawaii (Fig. 10c). This result closely matched the rainfall observations on Maui (Paakea, eastern Maui, reported 185 mm rainfall between 1700 UTC 2 March and 1700 UTC 3 March 1996) and Hawaii (cf. with Fig. 7d).

c. Frontal system of 13–14 November 1996

During the period of 0000 UTC 13 November–0000 UTC 14 November 1996, a cold front extending from a large extratropical low intensified as it moved southeastward toward the Hawaiian Islands. At 0000 UTC 14 November, the extratropical low, with a central pressure of 975 hPa, was centered at 34°N , 163°W (Fig. 11a), and the associated cold front was located to the east of the island of Kauai. A persistent northeast–southwest convective cloud band in the prefrontal region (Fig. 11b) brought heavy rainfall to portions of the western Hawaiian Islands. The largest amounts occurred on the island of Oahu, which recorded 24-h rain totals of more than 100 mm over most of the island (Fig. 11c), with

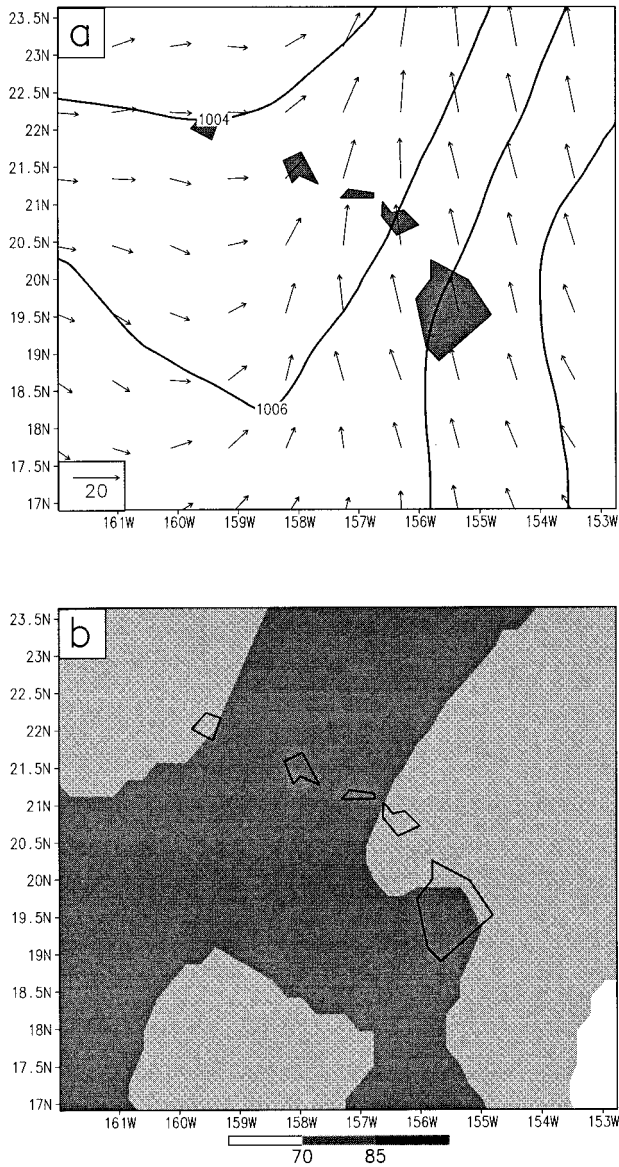


FIG. 12. AVN 24-h forecast valid at 0000 UTC 14 November 1996: (a) sea level pressure (hPa) and 1000-hPa winds (m s^{-1}); (b) 850-hPa RH (%).

a maximum amount of 205 mm observed at a site along the Koolau Range north of the city of Honolulu. The heavy rains that accompanied this and two other cold fronts during November 1996 made this month one of the wettest in history for the usually dry southwestern portions of Oahu.

For this case the AVN provided a good 24-h forecast of the development and propagation of the cold front. At 0000 UTC 14 November, cyclonic circulation associated with the low pressure system was in the western half of the domain, with southerly flow in the east. The forecast position of surface low was very close to the analyzed position. The 24-h predicted 850-hPa RH showed a moist region ($\text{RH} > 85\%$), with a width of

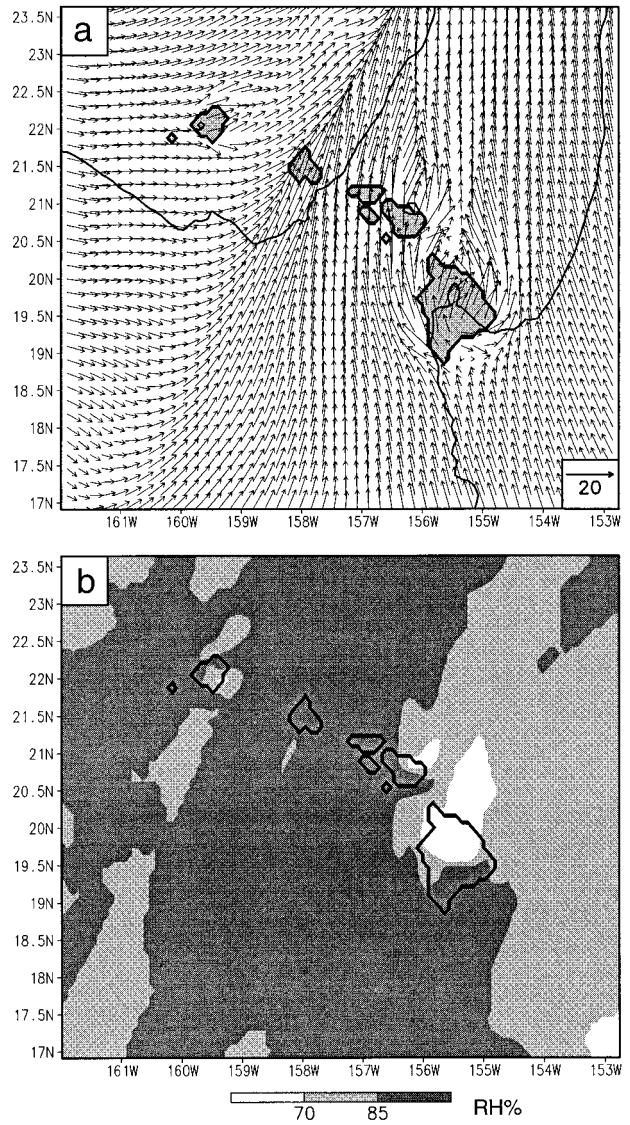


FIG. 13. Second nest RSM 24-h forecast valid at 0000 UTC 14 November 1996: (a) sea level pressure (hPa) and 1000-hPa winds (m s^{-1}), (b) 850-hPa RH (%), and (c) accumulated precipitation (mm) during the past 3 h.

270 km in the prefrontal region, which reasonably matched the cloud bands observed by satellite (Fig. 11b). Nevertheless, the AVN had difficulty resolving the mesoscale structure of the prefrontal convection and the interaction between the airflow and the complex island topography, thus limiting the usefulness of the AVN guidance for local weather forecasts.

The 24-h forecast by the second RSM nest shows a strong convergence zone at 1000 hPa near the island of Oahu, as southwesterly flow associated with the cold front converges with southerlies to the east (Fig. 13a). The band of high RH predicted by the second RSM nest (Fig. 13b) in the prefrontal region is wider (300 km) than that forecast by the AVN (Fig. 12b), with an ad-

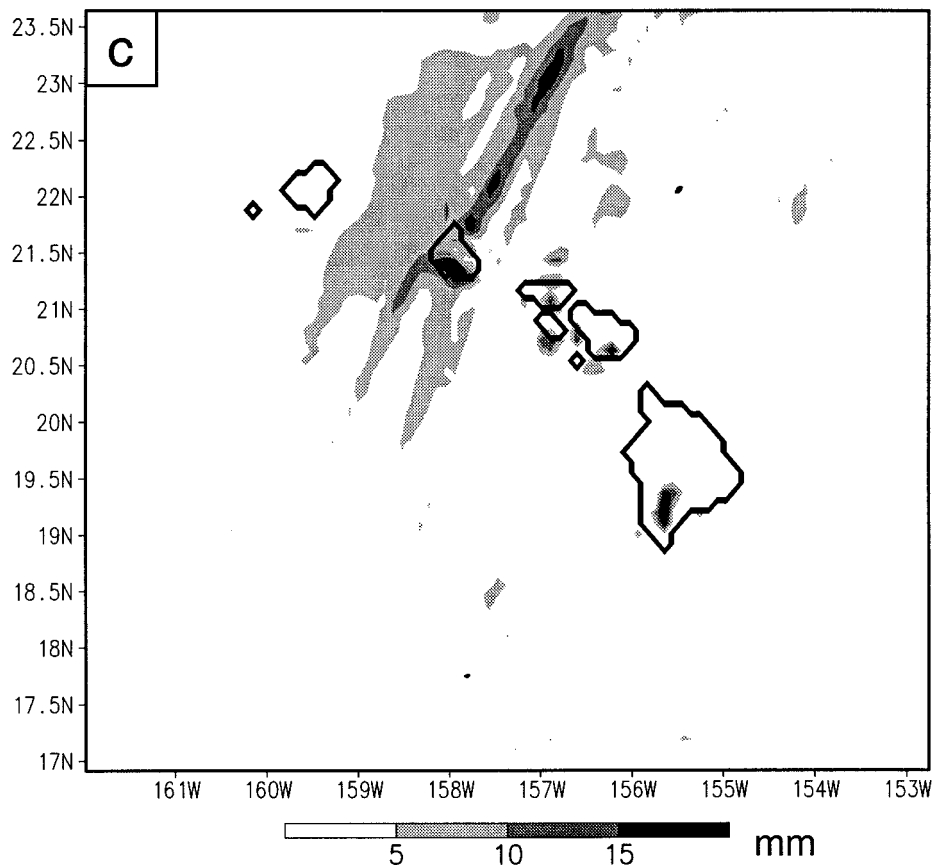


FIG. 13. (Continued)

ditional area with high RH ($>85\%$) forecast in the post-frontal region. For the islands of Maui, Hawaii, and Kauai, orographic lifting is apparent on the windward sides as evidenced by simulated high RH there (Fig. 13b). These regions include southern Hawaii, southwestern Maui, and western Kauai. Low RH is simulated on lee sides including over northern Hawaii, northeastern Maui, and eastern Kauai.

The heaviest rainfall was recorded over the southern half of Oahu during the period of 2100 UTC 13 to 0000 UTC 14 November. This is the region on the windward side of Oahu with pronounced large-scale low-level convergence during the frontal passage. It is apparent that during this period large-scale convergence is enhanced by orographic lifting over southern Oahu. The second RSM nest successfully forecast the 24-h rainfall accumulation with a heavy rainfall area across Oahu (not shown). The RSM also provides an accurate forecast of the location of the maximum rainfall during the 3-h period 2100 UTC 13 November to 0000 UTC 14 November. The area of the heaviest rainfall forecast by the RSM during this period is over southern Oahu, which experienced the heaviest rainfall and significant flooding at that time (Fig. 13c). The arrival time of the large-

scale convergence zone and the local effects are both well simulated by RSM for this particular case.

Although the AVN adequately forecast both the synoptic-scale and some of the larger mesoscale features in this case, the RSM still provided significantly better guidance for local weather conditions because of its ability to better resolve mesoscale weather features and the impact of topography.

4. Summary and future work

The NCEP regional spectral model (RSM) was implemented in Hawaii to provide mesoscale model guidance for operational weather forecasts in Hawaii. Three cases are presented in this paper to qualitatively evaluate the operational utility of the RSM model guidance. These cases are representative of Hawaiian cool season synoptic-scale disturbances that are responsible for most of the cool season heavy rain and high wind events in the Hawaiian Islands.

In each of the three cases presented, the synoptic-scale weather pattern was adequately forecast by the AVN. However, compared with AVN forecasts, the RSM simulations provide superior guidance for the lo-

cation of mesoscale convective rainfall and the impact of terrain on local weather in Hawaii. The case studies demonstrate that the RSM has the ability to simulate the interaction between the environmental airflow and the complex island topography. Low-level winds from the RSM show many of the mesoscale flow patterns observed in the vicinity of Hawaiian Islands. These include the 1) deceleration of incoming airflow upstream of island obstacles; 2) orographic lifting, causing a moist region on the windward side of the islands; and 3) flow splitting and acceleration around the islands, particularly over Maui and Hawaii, which have mountains above the trade wind inversion.

The model performance during disturbed weather conditions associated with synoptic-scale storm systems is encouraging. For the Kona storm case on 3 November 1995, the RSM prediction of a northeast-southwest-oriented rainband matches the convective cloud band observed in satellite imagery and radar data. Heavy rain was forecast for the island of Kauai, as observed, though the RSM missed the magnitude of the rains and location of the maxima on the north side of the island.

Comparisons with observations show a remarkably accurate simulation by the RSM for the cyclogenesis case on 3 March 1996. Major features such as the heavy rains and high winds over portions of Maui and Hawaii were successfully predicted. The RSM also performed well in forecasting the timing and distribution of heavy rainfall on the island of Oahu in the cold front case on 13 November 1996, demonstrating the potential utility of the RSM guidance for local weather forecasts in Hawaii.

Although the subjective comparisons between model output and observations led to the conclusion that the RSM is suitable for local weather forecasts in Hawaii, deficiencies in the model simulations were noted. For example, rainfall forecasts for Kauai in the kona low case were too low and the rainfall was not distributed in accordance with observations. As briefly discussed in section 3a, localized convection resulting from the effects of orography, which is an important consideration in Hawaii weather forecasts, should be better represented by a nonhydrostatic version of the RSM. Currently, the nonhydrostatic version of the RSM is undergoing tests at NCEP. For Hawaiian application, the nonhydrostatic version of the RSM, with a resolution of ~ 3 km, will be nested into the second hydrostatic RSM nest (Fig. 2).

Because of the lack of in situ observational data over the central Pacific Ocean, the enhancement of the initial conditions with remotely sensed and nonconventional data sources is a priority of the research agenda to improve future RSM simulations. The NCEP's spectral statistical-interpolation analysis system (Parrish and Derber 1992) has shown great improvement over the old optimal interpolation system. To apply this procedure directly to the regional domain, a 3D variational analysis is formulated on the physical grid and has been

tested for the RSM at NCEP (Wu and Juang 1996). With the 3D variational analysis, the nonconventional data will be incorporated into the initial conditions to make maximum use of the new data sources and will likely lead to better forecasts by the RSM in the future.

Three unconventional data sources are proposed to enhance the initial state of the RSM through application of the Regional Statistical Interpolation. These include the following.

- 1) The use of *GOES-9* derived moisture and wind data to provide important constraints for the RSM in data-sparse areas in the vicinity of Hawaii. Total column-integrated water vapor or precipitable water can be obtained from an algorithm based on a difference between the *GOES-9* 11- and 12- μm channels (e.g., Dalu 1986). The University of Wisconsin automated cloud-drift wind system uses a loop of three consecutive infrared window channel images to track the motion of clouds. A similar approach is used in their automated water-vapor motion wind system as it is applied to the water-vapor absorption channel images to track motion in the middle to upper atmosphere (e.g., Nieman et al. 1993).
- 2) WSR-88D radar data: low-level wind profiles and rain rates can be derived from a network of four WSR-88D radars on the islands of Hawaii, Kauai, and Molokai (Fig. 16 in Kodama and Businger 1998) and will be incorporated into the initial state of the nonhydrostatic island-scale nest of the RSM.
- 3) Global Positioning System (GPS) integrated water vapor data from an earth-based GPS receiver network: a network of continuously operating GPS receivers, including approximately 25 receivers outfitted with surface barometers, is currently being constructed across the state of Hawaii for a combination of geodetic and meteorological purposes (see Fig. 16 in Kodama and Businger 1998). The ability of GPS to accurately measure integrated water vapor and the utility of the resulting data in meteorological analysis is described in Businger et al. (1996). The integrated water vapor data will be used to enhance the initial state of the island-scale nest in the RSM, and the output of the model will be used in turn to evaluate the contribution of the GPS data to the accuracy of the simulation.

Due to the lack of conventional sounding sites in the Pacific region, surface analyses and 250-hPa analyses, which contain aircraft data from commercial flights will be used to verify the RSM output. Because of the importance of upper-level conditions on rainfall events in the subtropics (Li et al. 1997), successful simulation of 250-hPa flow by the RSM is crucial to correctly forecast these events. Cloud distributions and water vapor fields observed by satellites will be used to verify the midlevel moisture fields and 500-hPa pressure patterns in the RSM simulations. Gridpoint values of meteorological fields will be verified by nearby observations. In ad-

dition, the model-predicted rainfall distribution will be compared with observations from the Hawaiian rain gauge network and WSR-88D reflectivity data. Model-predicted total rainfall accumulation over individual basins will also be evaluated for flood forecasts.

Acknowledgments. This research is funded through a postdoctoral fellowship to Jian-Jian Wang, who performed the modeling study and wrote the draft of this paper under a cooperative agreement between the National Oceanic and Atmospheric Administration (NOAA) and the University Corporation for Atmospheric Research (UCAR). The authors wish to thank P. Jendrowski, H. Lau, and other members of the staff at the National Weather Service Forecast Office in Honolulu whose support made this work possible. Comments from three anonymous reviewers helped in the presentation of this paper.

REFERENCES

- Asselin, R. A., 1972: Frequency filter for time integration. *Mon. Wea. Rev.*, **100**, 487–490.
- Blumenstock, H. L., and S. Price, 1967: Climates of the United States Hawaii. *Climatography of the United States 60-51*, U.S. Dept. of Commerce, ESSA, 27 pp. [Available from NOAA Central Library, 2nd Floor, SSMC3, 1315 East-West Highway, Silver Spring, MD 20910.]
- Businger, S., and Coauthors, 1996: The promise of GPS in atmospheric monitoring. *Bull. Amer. Meteor. Soc.*, **77**, 5–18.
- , T. Birchard Jr., P. A. Jendrowski, K. Kodama, J. N. Porter, and J.-J. Wang, 1998: A bow echo and severe weather associated with a Kona low in Hawaii. *Wea. Forecasting*, **13**, 306–321.
- Chen, Y.-L., and A. J. Nash, 1994: Diurnal variation of surface airflow and rainfall frequencies on the island of Hawaii. *Mon. Wea. Rev.*, **122**, 34–56.
- , and J.-J. Wang, 1994: Diurnal variations of surface thermodynamic fields on the island of Hawaii. *Mon. Wea. Rev.*, **122**, 2125–2138.
- , and —, 1995: The effects of precipitation on the surface temperature and airflow over the island of Hawaii. *Mon. Wea. Rev.*, **123**, 681–694.
- Dalu, G., 1986: Satellite remote sensing of atmospheric water vapor. *Int. J. Remote Sens.*, **7**, 1089–1097.
- Garrett, A. J., 1980: Orographic cloud over the eastern slopes of Mauna Loa Volcano, Hawaii, related to insolation and wind. *Mon. Wea. Rev.*, **108**, 931–941.
- Haraguchi, P., 1977: Forecasting floods in Hawaii (excluding Hawaii island). NOAA Tech. Memo. NWSTM PR-16, 30 pp. [Available from NOAA/PRH, Grosvenor Center Mauka Tower, 737 Bishop St., Suite 2200, Honolulu, HI 96813.]
- Hong, S.-Y., and H.-M. H. Juang, 1996: Predictability study of heavy precipitation by using the NCEP regional spectral model. Preprints, *11th Conf. on Numerical Weather Prediction*, Norfolk, VA, Amer. Meteor. Soc., 22–23.
- Jorgensen, D. P., and M. A. LeMone, 1989: Vertical velocity characteristics of oceanic convection. *J. Atmos. Sci.*, **46**, 621–640.
- Juang, H.-M. H., 1996: Experimental daily weather forecast by the NCEP nonhydrostatic mesoscale spectral model. Preprints, *11th Conf. on Numerical Weather Prediction*, Norfolk, VA, Amer. Meteor. Soc., 166–167.
- , and M. Kanamitsu, 1994: The NMC nested regional spectral model. *Mon. Wea. Rev.*, **122**, 3–26.
- Kanamitsu, M., 1989: Description of the NMC global data assimilation and forecast system. *Wea. Forecasting*, **4**, 335–342.
- Kodama, K., and G. M. Barnes, 1997: Heavy rain events over the south-facing slopes of Hawaii: Attendant conditions. *Wea. Forecasting*, **12**, 347–367.
- , and S. Businger, 1998: Weather and forecasting challenges in the Pacific Region of the National Weather Service. *Wea. Forecasting*, **13**, 523–546.
- Leopold, L. B., 1949: The interaction of trade wind and sea breeze, Hawaii. *J. Meteor.*, **6**, 312–320.
- Li, J., Y.-L. Chen, and W.-C. Lee, 1997: Analysis of a heavy rainfall event during TAMEX. *Mon. Wea. Rev.*, **125**, 1060–1082.
- Nieman, S. J., J. Schmetz, and W. P. Menzel, 1993: A comparison of several techniques to assign heights to cloud tracers. *J. Appl. Meteor.*, **32**, 1559–1568.
- Parrish, D. E., and J. C. Derber, 1992: The National Meteorological Center's spectral statistical–interpolation analysis system. *Mon. Wea. Rev.*, **120**, 1747–1763.
- Ramage, C. S., 1962: The subtropical cyclone. *J. Geophys. Res.*, **67**, 1401–1411.
- Schroeder, T. A., 1977: Meteorological analysis of an Oahu flood. *Mon. Wea. Rev.*, **105**, 458–468.
- Simpson, R. H., 1952: Evolution of the Kona storm: A subtropical cyclone. *J. Meteor.*, **9**, 24–35.
- Smolarkiewicz, P. K., R. M. Rasmussen, and T. L. Clark, 1988: On the dynamics of Hawaiian cloud bands: Island forcing. *J. Atmos. Sci.*, **45**, 1872–1905.
- Uccellini, L. W., and D. R. Johnson, 1979: The coupling of upper and lower tropospheric jet streaks and implications for the development of severe convective storms. *Mon. Wea. Rev.*, **107**, 682–703.
- Wang, J.-J., and Y.-L. Chen, 1995: The characteristics of near-surface winds and thermal profiles on the windward side of the island of Hawaii. *Mon. Wea. Rev.*, **123**, 3481–3501.
- , and —, 1998: A case study of trade-wind rainbands and their interaction with the island-induced airflow. *Mon. Wea. Rev.*, **126**, 409–423.
- Wu, W.-S., and H.-M. H. Juang, 1996: A 3D variational analysis for the NCEP Regional Spectral Model. Preprints, *11th Conf. on Numerical Weather Prediction*, Norfolk, VA, Amer. Meteor. Soc., 86–87.